Sensorless position control of Permanent Magnet Synchronous Machines without Limitation at Zero Speed

Marco Linke, *Student Member*, Ralph Kennel, *Senior Member,* Joachim Holtz, *Fellow*

University of Wuppertal
Electrical machines and drives
http://www.ema.uni-wuppertal.de

Abstract — **Sensorless position control of Surface Mounted Permanent Magnet Synchronous Machines (SMPMSM) still is a challenge. High performance position control at low and zero speed is only possible using anisotropic effects being not considered in the fundamental-frequency machine models but in extended high-frequency models. This paper presents a new high-frequency injection method estimating the rotor position, which overcomes the small signal to noise ratio inherent to methods of this type published so far. This enables to track even small saliencies typical for SMPM synchronous machines. A small high-frequency voltage signal is injected into the rotor d-axis with no influence on the torque producing q-current. The demodulation of the responding high-frequency current signal is independent on machine parameters. Therefore the proposed method is independent on machine parameters and simply adaptable to different machines. As only the high frequency current has to be processed for position estimation, there is no additional hardware necessary besides that for standard drives with field oriented control.**

Index terms — **sensorless position control, high-frequency injection, anisotropic machine properties, signal modulation, surface mounted permanent magnet synchronous machine**

I. INTRODUCTION

Sensorless control schemes based on fundamental-frequency machine models fulfill demands in higher speed ranges. Position control as well as applications requiring permanent operation at low speeds cannot be obtained by these methods. This is owed to a loss of information on the rotor state when the induced rotor voltage becomes very small as the rotor speed reduces. The effect is not limited to a particular type of revolving field machines; it is associated with asynchronous machines as well as with synchronous machines.

An additional problem is the observer structure mostly used in fundamental estimation methods depending strongly on machine parameters. Particularly with asynchronous machines even small estimation errors in machine parameters add offsets of about half the slip depending on the accuracy of machine parameter estimation. Position estimation is generally impossible due to the scalar speed estimation when using fundamental state observers. Theoretically the position can be calculated by integrating the speed, but in practice the result will suffer under drift problems.

An interesting field of research relates to high performance sensorless position control of synchronous machines, which can be considered as more stringent requirement than just maintaining zero speed [1, 11]. It involves zero speed operation at a predetermined rotor position. Paper published recently indicate high-frequency injection methods becoming more and more attractive [1, 4, 5]. The absence of position sensors require the control algorithm to refer to anisotropic properties in salient ac-machines. Saliencies are not restricted to a specific machine type. They are well known in Synchronous Reluctance Machines as well as in Interior Permanent Magnet Machines, but they also exist - even if not dominating - in induction machines (rotor slots) and Surface Mounted Permanent Magnet Synchronous Machines.

Most methods published so far fail to track reliably small anisotropies in these types of AC machines. They suffer mainly under a small signal-to-noise ratio and a low spatial resolution. To expand the application area of high-frequency methods there is an increasing effort to design artificial saliencies in machines with originally small saliencies [2].

Most published methods which are able to track even small saliencies need additional voltage sensors [1, 12] and require high resolution detection of zero crossings of high frequency currents, which are difficult to detect in noisy environment [11] or require direct access to machine terminals for zero voltage detection [12]. Small saliencies increase the problem of precise voltage injection according to revolving high frequency signals - the nonlinear behavior of the inverter considerably decreases the estimation stability and position accuracy [9].

The method proposed in this paper presents some progress in overcoming the problems addressed above by using a new excitation method based on a high frequency amplitude modulation method. The method requires no additional hardware or sensors, and is insensitive to parameter variations as well as to additional parasitic saliencies that are not considered in the model.

II. HIGH-FREQUENCY INJECTION

High-frequency injection methods generally offer the possibility to observe the machine speed and/or position independent on the fundamental supply voltage and currents. Signal injection methods are suited to exploit machine properties that are neither considered in the fundamental machine state variables nor in the fundamental machine model. The high-frequency flux mainly propagates through the leakage paths in the stator and rotor. Due to the skin effect, however, the coupling of the high-frequency flux with the rotor is rather small and it is limited to regions close to the surface.

Some signal injection schemes use only current sensors, which are anyway necessary for field oriented control [2, 3]. Using the voltage injection principle instead of the current injection schemes, voltage sensors can be completely avoided. There are no requirements for additional hardware and for synchronization with the PWM pulse pattern as necessary in other methods [1, 12]. The absence of voltage sensors constitutes a major benefit of high-frequency injection methods.

In high-frequency methods, the physical effect used for position detection bases on machine anisotropies. A high-frequency signal gets modulated by the saliencies of the electrical machine. To detect that effect, it is possible to inject a voltage and monitor the current or to inject a current and to monitor the voltage. Due to the limited bandwidth of the current control loop it is preferred to inject a voltage, as it is done in the method proposed in this paper.

II. A. Representation of anisotropies in synchronous machines

Anisotropic machine behaviour results in different inductances with respect to a *dq*-reference frame that is synchronized with the rotor anisotropies. The flux induced by the high carrier frequency is mainly concentrated on the flux linkage through the leakage inductance:

$$\boldsymbol{l}_\sigma^{(\mathrm{A})} = \begin{bmatrix} l_{\sigma\mathrm{d}} & 0 \\ 0 & l_{\sigma\mathrm{q}} \end{bmatrix} \tag{2.1}$$

The inductance tensor $\boldsymbol{l}_\sigma^{(\mathrm{A})}$ represents high frequency leakage inductances in the reference frame aligned with the anisotropy. (marked with index $^{(\mathrm{A})}$)

A single dominant anisotropy, caused by the main flux, characterized by a single spatial cycle per pole pitch, is typical for SMPMSMs. This fact justifies the simplification to align the anisotropy with a field oriented *dq*-reference frame.

$$\boldsymbol{l}_\sigma^{(\mathrm{A})} = \boldsymbol{l}_\sigma^{(\mathrm{F})} \tag{2.2}$$

II. B. The basic structure of revolving high-frequency signal injection

The classical injected revolving voltage, creates a continues high frequency sinusoidal current usually called "carrier current". A rotating carrier signal according to [2, 10] can be created as

$$\boldsymbol{u}_\mathrm{c}^{(\mathrm{S})} = u_\mathrm{c}\, e^{\mathrm{j}\omega_\mathrm{c} t} \tag{2.3}$$

considering ω_c as carrier frequency. The index $^{(\mathrm{S})}$ refers to the stator coordinate system and u_c is the voltage amplitude

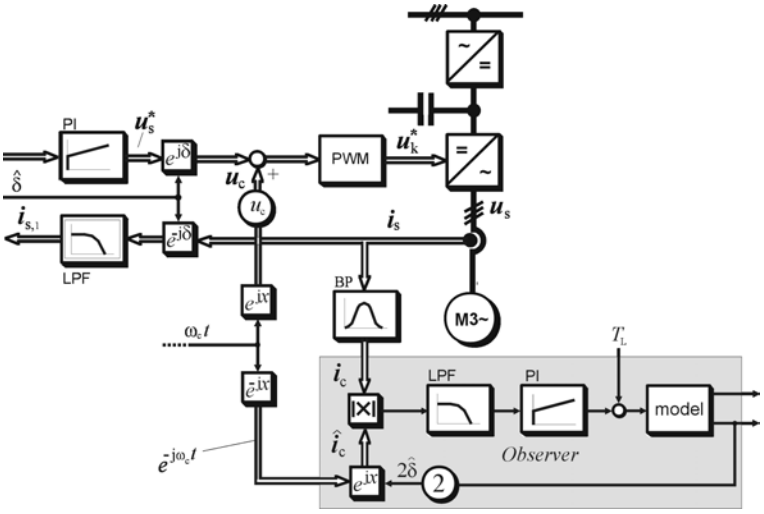

Fig.1: A basic structure of sensorless drive scheme using sinusoidal high-frequency injection with revolving carrier signal [2]

of the carrier signal superimposed to the fundamental voltage. The modulation of the injected high frequency signal by the machine anisotropies results in currents that are represented by the space vector $\boldsymbol{i}_\mathrm{c}$.

The high frequency components can be calculated by the differential stator equation in synchronous coordinates for high frequencies.

$$\boldsymbol{u}_\mathrm{c}^{(\mathrm{A})} = \boldsymbol{l}_\sigma^{(\mathrm{A})} \frac{d\,\boldsymbol{i}_\mathrm{c}^{(\mathrm{A})}}{dt} = u_c\, e^{\mathrm{j}(\omega_\mathrm{c}-\omega_\mathrm{a})t} \tag{2.4}$$

Consequently the voltage vector is modified by the angular velocity ω_a of the saliency. The resulting high–frequency current can be described as

$$\boldsymbol{i}_\mathrm{c}^{(\mathrm{A})} = -\mathrm{j}\frac{u_\mathrm{c}}{2(\omega_\mathrm{c}-\omega_\mathrm{a})l_{\sigma\mathrm{d}}l_{\sigma\mathrm{q}}} \begin{pmatrix} (l_{\sigma\mathrm{q}}+l_{\sigma\mathrm{d}})\mathrm{e}^{\mathrm{j}(\omega_\mathrm{c}-\omega_\mathrm{a})t} \\ +(l_{\sigma\mathrm{q}}-l_{\sigma\mathrm{d}})\mathrm{e}^{-\mathrm{j}(\omega_\mathrm{c}-\omega_\mathrm{a})t} \end{pmatrix}. \tag{2.5}$$

As the carrier frequency ω_c is chosen to be substantially higher than ω_a, the current can be described by (2.6), following a re-transformation to stationary coordinates.

$$\begin{aligned} \boldsymbol{i}_{\mathrm{c}}^{(\mathrm{S})} &= -\mathrm{j}\frac{u_{\mathrm{c}}}{2\omega_{\mathrm{c}} l_{\sigma\mathrm{d}} l_{\sigma\mathrm{q}}} \begin{pmatrix} (l_{\sigma\mathrm{q}} + l_{\sigma\mathrm{d}})\mathrm{e}^{\mathrm{j}\omega_{\mathrm{c}} t} \\ +(l_{\sigma\mathrm{q}} - l_{\sigma\mathrm{d}})\mathrm{e}^{-\mathrm{j}(\omega_{\mathrm{c}} - 2\omega_{\mathrm{a}})t} \end{pmatrix} \\ &= \boldsymbol{i}_{\mathrm{p}} + \boldsymbol{i}_{\mathrm{n}} \end{aligned} \tag{2.6}$$

In this equation, the positive current sequence component $\boldsymbol{i}_{\mathrm{p}}$, rotates at positive carrier frequency; it contains no information on the rotor position. The negative current sequence component $\boldsymbol{i}_{\mathrm{n}}$ rotates at an angular velocity $-\omega_c + 2\omega_a$ and contains the desired information concerning the angle $\omega_a t$ of the anisotropy.

The high frequency current component is separated by a bandpass filter from the fundamental frequency components and from the wide spread inverter frequency spectrum. Fig. 1 illustrates the basic principle.

The low pass filter eliminates the high-frequency current from the fundamental current inside the current control loop. An observer for the high frequency current processes the anisotropy model and provides rotor speed and position estimation.

III. PROPOSED AMPLITUDE MODULATED SPACE VECTOR METHOD

III. A. Derivation of the carrier signal

The carrier injection methods published so far suffer from some drawbacks. The poor signal-to-noise ratio and the parameter dependence of the observer to process the high frequency current reduce the sensitivity of the concept for small saliencies.

The new method generates a positive as well as a negative current sequence component, both containing information about the rotor position. The injected carrier voltage

$$\boldsymbol{u}_{\mathrm{c}}^{(\mathrm{S})} = u_{\mathrm{c}} \cos(\omega_{\mathrm{c}} t)\, e^{\mathrm{j}\hat{\delta}_a} \tag{3.1}$$

is always in alignment with the estimated position of the anisotropy (estimated values are marked with a hat ^):

$$\hat{\delta}_{\mathrm{a}} = \hat{\omega}_{\mathrm{a}} t\ . \tag{3.2}$$

The anisotropy in a SMPMSM is mainly based on the saturation effect of the main flux; it rotates at the same frequency ω as the rotor. The subscript $_{\mathrm{a}}$ generally indicates an anisotropy-aligned coordinate system as opposed to the field oriented system. Both coincide in the case of surface mounted PMSM. A transformation of the carrier voltage to field coordinates is done by multiplying (2.3) by $e^{-\mathrm{j}\delta}$.

This leads to

$$\boldsymbol{u}_c^{(\mathrm{F})} = u_{\mathrm{c}} \cos(\omega_{\mathrm{c}} t)\, e^{\mathrm{j}(\hat{\delta}-\delta)}\ . \tag{3.3}$$

The differential equation (3.4) is similar to (2.4).

$$\boldsymbol{u}_c^{(\mathrm{F})} = u_{\mathrm{c}} \cos(\omega_{\mathrm{c}} t)\, e^{\mathrm{j}(\hat{\delta}-\delta)} = \boldsymbol{l}_{\sigma}^{(\mathrm{F})} \frac{d\,\boldsymbol{i}_{\mathrm{c}}^{(\mathrm{F})}}{dt} \tag{3.4}$$

Stator resistance, induced voltage and cross coupling of the currents are neglected in the differential stator equation similar to (2.5). This is only permitted if the carrier frequency ω_c is much higher than the fundamental frequency. The real field angle δ is the unknown variable in this equation.
The solution in field coordinates of (3.4) is

$$\boldsymbol{i}_{\mathrm{c}}^{(\mathrm{F})} = \frac{u_c}{\omega_c} \sin\omega_c t \left(\frac{1}{l_{\sigma\mathrm{d}}} \cos(\hat{\delta}-\delta) + \mathrm{j}\frac{1}{l_{\sigma\mathrm{q}}} \sin(\hat{\delta}-\delta) \right). \tag{3.5}$$

The transformation to stationary coordinates results in

$$\begin{aligned} \boldsymbol{i}_{\mathrm{c}}^{(\mathrm{S})} &= u_{\mathrm{c}}\ \frac{1}{\mathrm{j}4\,\omega_{\mathrm{c}}\, l_{\sigma\mathrm{d}}\, l_{\sigma\mathrm{q}}} \begin{pmatrix} \left[(l_{\sigma\mathrm{d}} + l_{\sigma\mathrm{q}})\, e^{\mathrm{j}(\omega_{\mathrm{c}} t + \hat{\delta})} - (l_{\sigma\mathrm{d}} - l_{\sigma\mathrm{q}}) e^{\mathrm{j}(\omega_{\mathrm{c}} t - \hat{\delta} + 2\delta)} \right] + \\ \left[-(l_{\sigma\mathrm{d}} + l_{\sigma\mathrm{q}}) e^{\mathrm{j}(-\omega_{\mathrm{c}} t + \hat{\delta})} + (l_{\sigma\mathrm{d}} - l_{\sigma\mathrm{q}}) e^{\mathrm{j}(-\omega_{\mathrm{c}} t - \hat{\delta} + 2\delta)} \right] \end{pmatrix} \\ &= \boldsymbol{i}_{\mathrm{p}} + \boldsymbol{i}_{\mathrm{n}} \end{aligned} \tag{3.6}$$

The analysis of the spectral components of the stator current provides some interesting results.

III. B. Analysis of the high-frequency current

The stator current described by (3.6) can be separated in a positive sequence component $\boldsymbol{i}_{\mathrm{p}}$ and a negative sequence component. Other than the current in (2.6), also the positive sequence component contains information about the field position angle δ. The information content of the frequency spectrum increases.

Figure 2 illustrates the frequency spectrum of the currents (3.6). The negative and positive frequency range contain

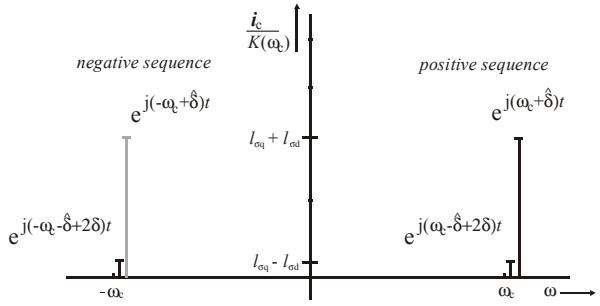

Fig. 2: Complex frequency spectrum of the high frequency current $\boldsymbol{i}_{\mathrm{c}}$ according to 3.6 for small saliencies

field angle information, the amplitude of which is proportional to the difference of *d*- and *q*-leakage inductances. The former intuitive assumption of small anisotropies ($l_{\sigma q}$ - $l_{\sigma d}$) being directly related to a low-amplitude information content in the positive and negative sequence components is hereby confirmed (Fig. 2)

It is evident from (3.5) that the imaginary part of the high frequency current decreases when the estimated angle approaches the real field angle and finally becomes zero. Hence the harmonic torque distortion due to the test signal is negligible.

IV. DEMODULATION OF THE CARRIER SIGNAL

Using high frequency injection methods for sensorless control, the signal demodulation constitutes a major demand for signal processing. To reduce the calculation, the high-frequency current $\boldsymbol{i}_c$ (3.6) is transferred to a reference frame in a negative direction at approximate carrier frequency. This is done by

$$\boldsymbol{i}_c^{(\omega_c t+\hat{\delta})} = \boldsymbol{i}_c^{(S)}\, e^{-j(\omega_c t+\hat{\delta})} \tag{4.1}$$

This transformation generates a high frequency current signal that is easy to demodulate without referring to machine parameters. Assuming the remaining negative sequence current components of $\boldsymbol{i}_c$ is rejected by a low pass filter, transformation (4.1) applied to the current signals (3.6) results in

$$\boldsymbol{i}_p^{(\omega_c t+\hat{\delta})} = u_c \;\; \frac{1}{j4\,\omega_c\, l_{\sigma d}\, l_{\sigma q}} \begin{bmatrix} (l_{\sigma d}+l_{\sigma q}) \\ -(l_{\sigma d}-l_{\sigma q}) e^{j(2\delta-2\hat{\delta})} \end{bmatrix}. \tag{4.2}$$

It can easily be separated because it is transformed by (4.1) to about twice the carrier frequency.
Equation 4.2 illustrates the current response containing the useful information about the misalignment of the estimated field angle with reference to the real field angle. It can be regarded as an error estimation angle

$$\Delta\delta = \delta - \hat{\delta}\,. \tag{4.3}$$

The current response is further simplified to reduce processing power necessary for demodulation. In the case of small error estimation angles the current response is:

$$\boldsymbol{i}_p^{(\omega_c t+\hat{\delta})} = u_c \;\; \frac{1}{4\,\omega_c\, l_{\sigma d}\, l_{\sigma q}} \begin{bmatrix} -j(l_{\sigma d}+l_{\sigma q}) \\ -(l_{\sigma d}-l_{\sigma q})\, 2\,\Delta\delta \end{bmatrix} \tag{4.4}$$

This equation shows the real part of the current response in the reference frame according to (4.1) being proportional to the error angle $\Delta\delta$. This is used to track the field angle by a closed loop tracking system. The basic principle of adjusting the carrier voltage to the estimated anisotropy angle is possible and proved by equation (4.2).

To increase the overall sensitivity of the sensorless concept, the same demodulation method as described above for the positive current component of equation (2.6) can be applied to the negative current sequence component.

$$\boldsymbol{i}_c^{(-\omega_c t+\hat{\delta})} = \boldsymbol{i}_c^{(S)}\, e^{j(\omega_c t-\hat{\delta})} \tag{4.5}$$

The result is similar to (4.4) with the difference that the negative frequency range be exploited for tracking the field angle. Using both signals (4.1) and (4.5) decreases the possible errors and tolerances when processing the rotor position.

V. SENSORLESS POSITION CONTROL OF SMPMSM

As discussed in Chapter IV, a complex demodulation of the carrier can be replaced by tracking the error estimation signal (4.3). The theoretical evaluation confirms that it is possible to generate a calculation quantity representing the misalignment $\Delta\delta$ between the estimated field angle and its true value, (4.4). Tracking an error signal is robust against noise and measurement tolerances e.g. the limited resolution of the analog to digital converter in drive controllers. As the *estimated field error angle* $\Delta\delta$ is evaluated in the proposed method instead of *field angle* itself, the resolution of the high frequency current signal $\boldsymbol{i}_c$ is less critical. The error signal $\Delta\delta$ is as an incremental variable that changes only slowly in comparison to the sample frequency.

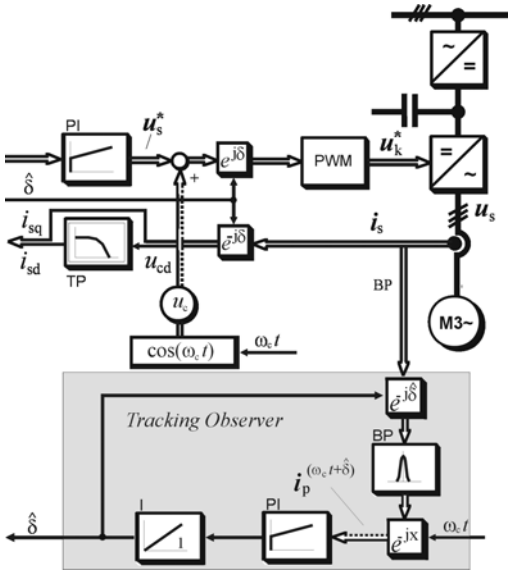

Fig.3: Signal flow graph of the field angle estimation scheme based on the proposed method

The signal flow graph in Figure 3 illustrates the basic structure of the proposed sensorless scheme. The positive sequence current in (4.4) has a real component proportional to the error angle $\Delta\delta$. This signal is sampled at the sampling frequency of the current control loop. The following PI-controller feeds a controlled oscillator to create the estimated field angle. This results in a closed loop structure that corrects the field angle in each sampling cycle. A high sampling frequency ensures good and dynamically fast alignment with field axis. The disturbances of the acquired signal are low, thus permitting operation at low carrier amplitudes. The prominent advantage is that the tracking observer does not require any machine parameters.

To establish narrow filter characteristics, the current $\boldsymbol{i}_c$ in Fig. 3 is transformed to the estimated field coordinate system by

$$\boldsymbol{i}_c^{(\hat{\delta})} = \boldsymbol{i}_c^{(S)}\, e^{-j(\hat{\delta})}. \tag{5.1}$$

This transformation results only in current components of carrier frequency ω_c. This allows using narrow band filters that reject all frequencies except the carrier frequency, which is essential to estimate small saliencies[1].

VI. Experimental Results

The field axis is fixed to the rotor only at noload; therefore the rotor position can be then derived from the estimated field angle. However, a small difference exists between both angles when a load is applied. A linear compensation related to the torque current reduces this effect substantially. The estimated rotor field angle is therefore considered in alignment with the rotor position angle.

Experimental results were obtained using a commercial 6-pole SMPMSM servo drive (see Table 1):

Table 1: technical data SMPMSM

Rated power	1.2 kW
Rated speed	6000 rpm
Rated voltage	400 V
Rated current/ max. current	2,8 A/ 15.2 A

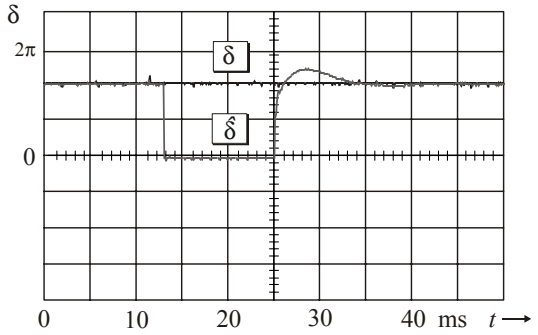

Fig.4: Step response of the field tracking system, measured rotor position δ and estimated rotor angle $\hat{\delta}$ after forced reset to zero

The switching frequency is 8 kHz, the carrier frequency is 2 kHz with a peak carrier current $i_{c,.max}$ of 200 mA. The current is processed by the same standard 12-Bit A/D converter used for sensing the fundamental currents. The saliency ratio in this machine is small, reflected in a leakage inductance ratio of:

$$\frac{l_{\sigma d}}{l_{\sigma q}} \approx 0.9 \tag{6.1}$$

In comparison to that, an isotropic machine has an inductance ratio close to 1. Small saliencies require a highly sensitive estimation method, which must be robust against parasitic anisotropies like inverter clamping effects [9].

The high carrier frequency ensures a high dynamic bandwidth of the estimation method, which is necessary for servo drive applications. Fig. 4 illustrates the response of the field tracking control loop after forcing the estimation angle to zero.

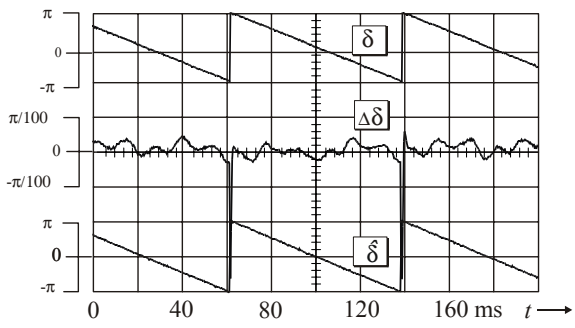

Fig.5: Measured rotor position δ and position error $\Delta\delta$ between the measured and estimated position, estimated position (half of rated load, steady state operation)

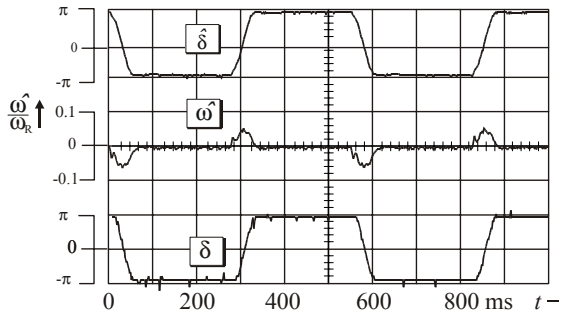

Fig.6: Response to commanded step changes of one full revolution. Only the estimated position and estimated rotor speed are used for drive control, while the measured position δ is only a reference

For evaluating the accuracy of the sensorless position identification method, steady-state tests were performed. The

field tracking control is based on a PLL structure (Fig. 3). Therefore it is free of phase lags at steady-state operation. The accuracy and resolution of the sensorless position estimation method is illustrated in Fig. 5.

Positioning applications require repeatable operation to predetermined angular rotor positions. Fast dynamic position control is necessary to provide that the method offers repeatable dynamic positioning operation without sensing the position even with rated load (Fig.6).

The proposed high-frequency method is mainly applicable to operation at low fundamental frequencies. Fig. 7 shows a positioning test. During the operation the drive operates at a fundamental frequency of 60 Hz. This is possible, because the filter characteristic of the narrow band pass filter separates the high frequency components from noise and the fundamental frequency.

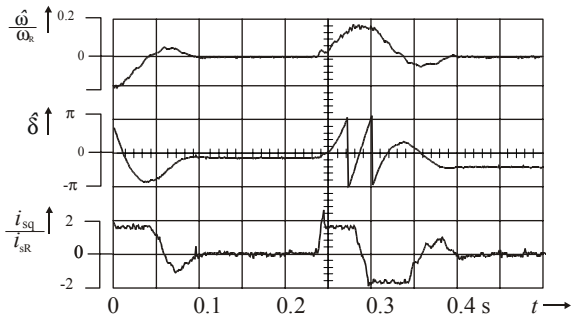

Fig.7: Sensorless positioning, estimated position and estimated rotor speed are used for drive control, the current i_{sq} is limited to twice the rated current i_{sR} .

VII. CONCLUSION

This paper presents a new sensorless control algorithm for Surface Mounted Permanent Magnet Synchronous Machines using high frequency voltage injection. The method is able to track even small saliencies in electrical machines. The injection of amplitude modulated carrier signals, as an overlay to the fundamental frequency, offers a highly sensitive saliency detection method. With respect to anisotropies caused by saturations, the maximum flux density occurs in direction of the d-axis of a field oriented coordinate system and can be regarded as fixed to the rotor. Therefore the estimation of rotor position basically results in detecting the flux angle and modeling the phase shift between them. Considering this, the method is independent of machine parameters as only a position error is estimated and tracked by close loop observer. The experimental results verify this method to detect reliably even small saliencies in SMPMSM and exploit them for high dynamic position control. The method provides main advantages at low and zero speed.

REFERENCES

[1] J. Holtz, Sensorless Position Control of Induction Motors - an Emerging Technology, IEEE Transactions on Industrial Electronics, Vol. 45, No. 6, December 1998.

[2] Robert D. Lorenz, Sensorless Drive Control Methods for Stable, High Performance, Zero Speed Operation, International Conference on Power Electronics and Motion Control- EPE-PEMC, Kosice 2000.

[3] J.K Ha, S.K. Sul, K. Ide, I. Murokita, K. Sawamura, Physical Understanding of High Frequency Injection Method to Sensorless Drives of an Induction Machine, IEEE-IAS 2000, Conference Record of the 2000 IEEE Ind. Appl. Conference, Vol.4

[4] J.K. Ha, S.K. Sul, Sensorless Field-Orientation Control of an Induction Machine by High-Frequency Signal Injection, IEEE Tran. On Ind. Appl., Vol. 35. No.1, Jan./Feb. 1999

[5] A.Consoli, F. Russo, A. Testa, Low- and Zero-Speed Sensorless Control of Synchronus Reluctance Motors, IEEE Trans. On Ind. Appl., Vol.35, No.5, Sept./Oct. 1999,pp.1050-1050

[6] J. Holtz, The Dynamic Representation of AC Drive Systems by Complex Signal Flow Graphs, *Conf. Record of ISIE (International Symposium on Industrial Electronics)*, Santiago de Chile, Chile, 1994, pp. 1-6

[7] M.Schroedl, Sensorless control of AC Machines at Low Speed and Standstill based on the "INFORM" Method, IEEE Ind. Appl. Society Annual Metting, Pittsburgh, Sept.30- Oct. 4, 1996, pp 270-277

[8] N. Teske, G. M . Asher, M. Sumner, K.J. Bradley, Suppression of Saturation Saliency Effects for the Senorless Position Control of Induction Motor Drives under loaded Conditions, IEEE Trans. on Ind. Elec., Vol. 47, No. 5, Sep/Oct. 2000, pp 1142-1149

[9] N. Teske, G.M Asher, K.J. Bradley, M.Sumner, Analysis and Suppression of Inverter Clamping Saliency in Sensorless Position Controlled Induction Motor Drives, IEEE Ind. Appl. Society Annual Meet., Chicago, Sept. 30 –Oct. 4, 2001

[10] F. Briz, M.W. Degner, A. Diez, R.D. Lorenz, Static and Dynamic Behaviour of Saturation-Induced Saliencies and theri Effect on Carrier Signal Based Sensorless AC Drives, IEEE Ind. Appl. Society Annual Meet., Chicago, Sept. 30 – Oct. 4, 2001

[11] A. Consoli, G. Scarcella, A. Testa, Industry Application of Zero-Speed Sensorless Control Techniques for PM Synchronous Motors, IEEE Trans. on Ind. Appl., Vol. 37, No.2, March/April 2001

[12] A. Consoli, G. Scarcella, A. Testa, A New Zero Frequency Flux Detection Approach for Direct Field Oriented Control Drives, IEEE Trans. on Ind. Appl., Vol. 36, No.3, May/June 2000, pp. 797-804